Journal of Alloys and Compounds 480 (2009) 942–946

Contents lists available at ScienceDirect

Journal of Alloys and Compounds

journal homepage: www.elsevier.com/locate/jallcom

Synthesis of single phase rhombohedral $LaNiO_3$ at low temperature and its characterization

Mridula Biswas*

Naval Materials Research Laboratory, Addl. Ambernath, Thane-421506, India

ARTICLE INFO

Article history:
Received 13 November 2008
Received in revised form 18 February 2009
Accepted 21 February 2009
Available online 5 March 2009

Keywords:
Ceramics (A)
Oxide materials (A)
Chemical synthesis (B)
Crystal structure (C)
X-ray diffraction (D)

ABSTRACT

$LaNiO_3$ powder was prepared by gel combustion method using sucrose as fuel. Differential thermogravimetry coupled with differential scanning calorimetry (DTA-DSC) was used to identify the combustion temperature and the weight loss regime. The powders calcined at various temperatures were characterized by X-ray diffractometry (XRD), specific surface area analysis, UV-diffused reflectance spectroscopy (UV-DRS), transmission electron microscopy (TEM) and scanning electron microscopy (SEM). The XRD data revealed the formation of phase pure rhombohedral $LaNiO_3$ at temperature as low as 750 °C without formation of any intermediate compound. Local sintering of the crystallites increased in a monotonic manner when calcination temperature increased. Specific surface area showed a decreasing trend with increase in calcination temperature. Band gap studies in the UV–visible range of the optical spectrum were carried out for the powders calcined at various temperatures. Phase pure rhombohedral $LaNiO_3$ showed no optical absorption in this range. SEM study revealed the porous nature of the calcined powder.

1. Introduction

Lanthanum nickelate is used as an electrode material in electronic device such as FERAM since it has the property to conduct electricity [1]. This material shows narrow band metallic conductivity down to 1.5 K while other compounds with Pr, Nd, Sm and Eu in place of La of $RNiO_3$ group shows metal–insulator transition and an antiferromagnetic transition at higher temperature [2,3]. It also shows Pauli-paramagnetism [4]. Lanthanum nickelate presents the most favorable combustible sensing electronic properties at gas concentration larger than 2000 ppm from about 250 to 350 °C in oxidizing atmosphere. There are two wide markets for this material: (1) to sense the coal gasification product stream with very high pressure at above 600 °C and (2) to control the combustion in near stoichiometric air/fuel mixtures of car engines [5]. In addition, Hamada suggested that this material can be utilized as a superconductor in future [2]. Lanthanum nickelate is a ternary oxide of rhombohedrally distorted perovskite structure. In this material Ni adopts its higher oxidation state which is stabilized at lower temperature. So there is a real need to synthesize this material at lower temperature than the temperature required for solid state synthesis method [6–8].

The production of high-performance ceramics, which display such properties, has driven forward the elaboration of new powder synthesis routes. Single phase $LaNiO_3$ was synthesized using a number of methods including conventional ceramic powder technology, nitrate decomposition, pechini method, hydrothermal flow coprecipitation, coprecipitation, to name a few [9–14]. Those techniques generally require high temperatures (in excess of 750 °C), flowing oxygen and long calcination periods (usually in excess of 2 h) in order to obtain single phase $LaNiO_3$.

Combustion synthesis is a promising route for faster production of ultrafine ceramic powders [15]. Combustion synthesis is of two types, solution combustion synthesis and gel combustion synthesis. In the former method, the solution of composite metal nitrates and fuel is heated in a muffle furnace at about 500 °C to initiate the combustion reaction. The fuels used are urea, glycine, oxalyl dihydrazide, etc. [16–19]. In the later method, a solution of composite metal nitrates and fuels such as citric acid, urea formaldehyde, sucrose, etc. is heated on a hot plate to form a gel [20–26]. The gel undergoes auto-combustion to form either the required ceramic phase on hot plate itself if the heat generated is sufficiently high to overcome the requirement for activation energy for the phase formation of ceramic powders or its precursor [27–29]. Otherwise, the precursor powder is further calcined to form required crystalline phase and eliminate the remaining carbon particles which do not go off during combustion. Combustion synthesis produces weakly agglomerated fine particles that can be ground easily [30]. Sinteractivity of ultra fine powders prepared by combustion synthesis is very high at much lower temperature due to the rapid diffusion among the solids [31,32]. Preparation of lanthanum nickelate nanopowder has been reported by several authors using citric acid

* Tel.: +91 2512621950; fax: +91 2512620604.
E-mail address: luckymridula@yahoo.com.

0925-8388/$ – see front matter © 2009 Elsevier B.V. All rights reserved.
doi:10.1016/j.jallcom.2009.02.099

and ethylene glycol and glycine as fuel [33,34]. Sucrose has been used as fuel for combustion synthesis of various nanocrystalline ceramic powders. The present paper focuses on the phase transformation, lattice distortion and band gap studies of lanthanum nickelate nanopowders prepared by combustion synthesis using sucrose as the complexing agent and fuel for combustion. The lanthanum nickelate powder prepared was also characterized for crystallite size and surface area and the results were discussed.

2. Experimental procedure

Lanthanum nitrate ($La(NO_3)_3{\cdot}6\,H_2O$) and nickel nitrate ($Ni(NO_3)_2{\cdot}9H_2O$) of 99% purity were procured from Central Drug House (P) Ltd., New Delhi. Sucrose (Merck, India) and nitric acid (Merck, India) of analytical reagent grade were used as received. Doubly distilled water was used for preparation of solutions. The procedure for sucrose combustion synthesis is reported elsewhere [25]. Stoichiometric amount of lanthanum nitrate and nickel nitrate were dissolved in water to form a homogeneous solution. Sucrose was then dissolved in the solution in a proportion of two moles per mole of metal ion. The resulting transparent solution was heated on a hot plate until it turned into a black gel. The gel was subsequently heated on the hot plate to set an exothermic self-sustaining smoldering type of combustion reaction. Fig. 1 shows the flow chart of the sucrose combustion process. Differential scanning calorimetry coupled with thermogravimetric analysis (DSC-TGA) (Setsys 16/18, Setaram Scientific and Industrial Equipment, France) of the gel was carried out at a heating rate of 10 °C to 800 °C. The combustion product was calcined at various temperatures from 500 to 800 °C for 2 h. The crystalline structure and phase purity of the obtained powders were analyzed by X-ray diffractometry (XRD) (Xpert MPD, PAnalytical B. V., Almelo, the Netherlands) using Cu Kα radiation in the angular region of $2\theta = 20^\circ$–80° with a step size of 0.005°. The observed XRD data were processed to obtain the exact peak positions to determine crystallite size [20]. The following calibration equation was generated using least square method:

$$\Delta 2\theta = a_1 + a_2 \cos\theta_{obs} + a_3 \sin 2\theta_{obs}$$

where $\Delta 2\theta$ is the deviation from the observed angle, $2\theta_{obs}$, the three constants, a_1, a_2 and a_3 were calculated from the data obtained using silicon standard sample. Average crystallite size was calculated from XRD data using Debye–Scherrer relation, $D = 0.94\lambda/\beta\cos\theta$, where D is the crystallite size, λ is the wavelength of Cu Kα radiation (1.5406 Å), β is full width at half maxima (FWHM) of the broadening of the diffraction line and θ was obtained after correcting the observed peak position. Instrumental broadening was eliminated from the raw XRD data using the following equation:

$$\beta = \sqrt{(\beta_m^2 - \beta_s^2)}$$

β_s is the system broadening which was found using a polycrystalline silicon standard sample and β_m is the observed broadening in the XRD raw data of the powders [35].

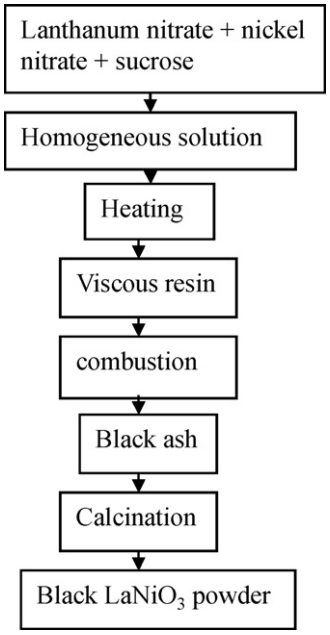

Fig. 1. Process flow chart.

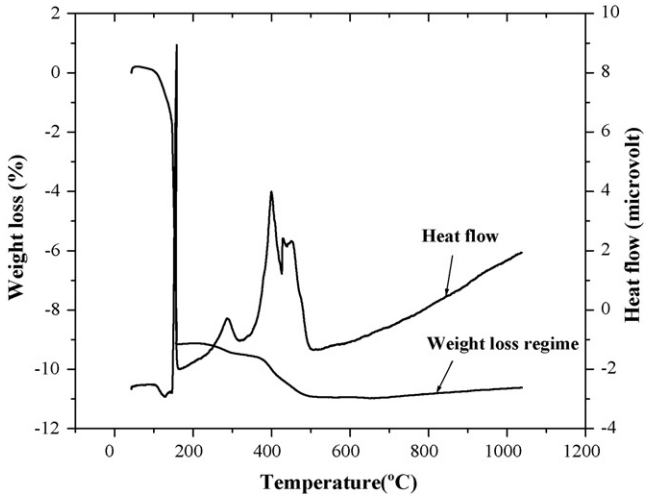

Fig. 2. DTA–TGA Diagram.

Specific surface area analysis (Sorptomatic 1990, Thermo Fennigan, Radano (MI), Italy) of the powders calcined at various temperatures was carried out by Brunauer–Emmett–Teller (BET) method. Average particle sizes of the powders were calculated using the relation, $D_{av} = 6/(S_w \times \rho)$, where S_w is the specific surface area, ρ is the density and D_{av} is the average diameter of the particles, assuming that all the particles were spherical.

Band gap studies were carried out by diffused reflectance spectroscopy (DRS) using UV-DRS spectrophotometer (VARIAN, Cary 500 Scan and Labsphere, Model No. DRA-CA-5500, North Sutton, NH) at 27 °C in the wavelength range of 200–700 nm. Band gaps were calculated using the optical frequency at the onset of direct photon transition. Corresponding wavelengths at the threshold of the direct photon transition have been used in the relation $E_g = \hbar\omega_g$, where E_g is the band gap between the band edges of conduction and valance bands, $\hbar$ is the modified Plank's constant and ω_g is the frequency at the threshold of direct photon transition. Microstructure of the as-calcined powder was observed under scanning electron microscope (SEM) (LEO1455, Oxford Instruments, UK).

The $LaNiO_3$ prepared by calcination of the combustion product was found to comprise of soft agglomerates of fine particles. These agglomerates were broken down into fine particles by planetary ball milling in isopropanol medium for 12 h using zirconia grinding media. A charge to ball ratio of 1:4 by weight was used during milling. TEM (Philips USA) analysis of the $LaNiO_3$ powder was carried out to find the morphology and crystallite size.

3. Results and discussion

The solution containing stoichiometric amount of lanthanum nitrate and nickel nitrate showed a pH nearly 1 due to dissolution of the nitrates. The reaction between the metal nitrates and sucrose was explained by Bose and Wu [25]. At this acidic pH, sucrose

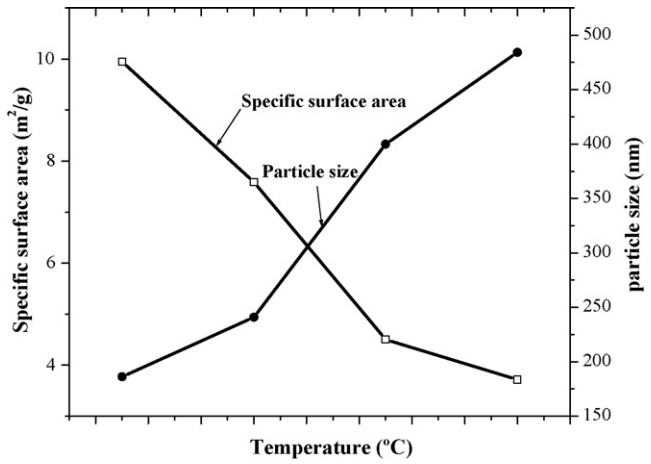

Fig. 3. Plot of surface area and particle size vs. temperature.

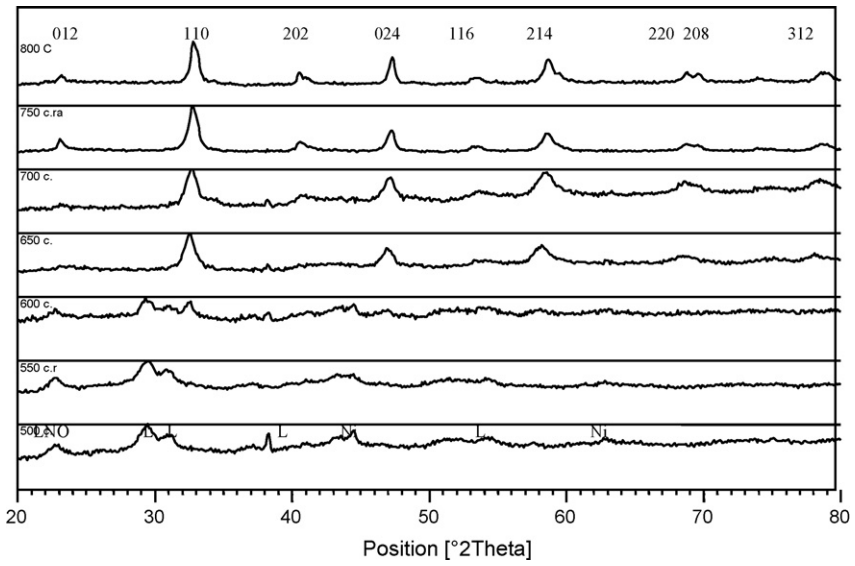

Fig. 4. XRD plot of powder at temperatures from 500 to 800 °C, where L indicates lanthanum oxide, LNO lanthanum nickelate and Ni nickel oxide.

undergoes polymerization to form a dark viscous resin and the lanthanum and nickel ions form co-ordinate bond with the hydroxyl groups present in the polymer. This resin transformed to a black gel which burnt on the hot plate itself. Fig. 2 shows the DTA–TGA plot of the gel. Two exotherms are observed at temperatures of 160 °C and 350–525 °C. The sharp exotherm observed at 160 °C indicates the sudden charring of sucrose polymer. The broad exotherm observed in the temperature range of 350–525 °C corresponds to the slow combustion of carbon. TGA shows weight loss up to 525 °C indicating complete removal of organic matters took place at temperature below 525 °C. The surface area of the combustion product decreased from 9.95 to 3.72 m^2/g when calcination temperature increased from 650 to 800 °C. Particle size calculated from the surface area data increased from 186.2 to 484.2 nm when calcination temperature increased from 650 to 800 °C. Fig. 3 shows variation of surface area and particle size with calcination temperature of the lanthanum nickelate powder.

Fig. 4 represents the evolution of the peaks in the XRD patterns for $LaNiO_3$ powders calcined at various temperatures. There was evolution of some crystalline phases at 500 and 550 °C and were identified as oxygen deficient phases. These phases observed were $LaNiO_{2.7}$, $LaNiO_{2.5}$ and La_2NiO_4 according to the JCPDS file no. 37-0928, 82-0556, 78-2186, 82-2176, 80-1914, 14-0481, 83-1355. Presence of free nickel oxide and lanthanum oxide were observed at 500 °C. But at 600 °C there was no trace of free nickel oxide and lanthanum oxide. $LaNiO_{2.5}$ and $LaNiO_{2.7}$ correspond to the tetragonal and triclinic crystal structures, respectively [34]. XRD patterns indicate that crystallization of $LaNiO_3$ phase starts at 600 °C. Thus the powder calcined at 600 °C has the composition range varied from $LaNiO_{2.5}$ in which one of six anionic sites is vacant to $LaNiO_3$, a compound with a complete anionic sub lattice. This is called brownmillerite structure [36]. Most of the cations in the first transition row are involved in formation of these types of oxygen deficient phases because these cations are able to adopt both octahedral and tetrahedral voids in a structure. A homologous series of general formula $A_nM_nO_{3n-1}$ is obtained, where $n-1$ layers are of octahedral structure with a single layer of tetrahedral structure along *b* axis [37,38]. At the same time another discovery was made that M cations are able to adopt five co-ordinations, ordered structure based on interconnected MO_6 octahedra with MO_5 square pyramids [39]. It was observed that oxygen deficiency decreased as the temperature of calcination increased. Strong characteristic peaks of rhombohedral $LaNiO_3$ along with very little trace of monoclinic

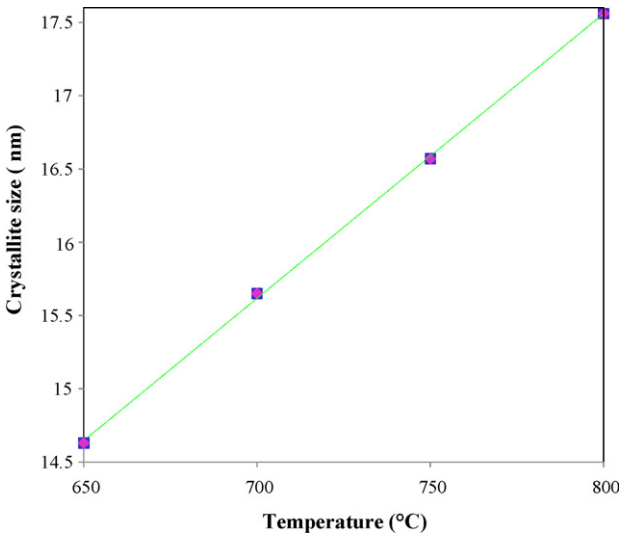

Fig. 5. Plot of temperature vs. crystallite size.

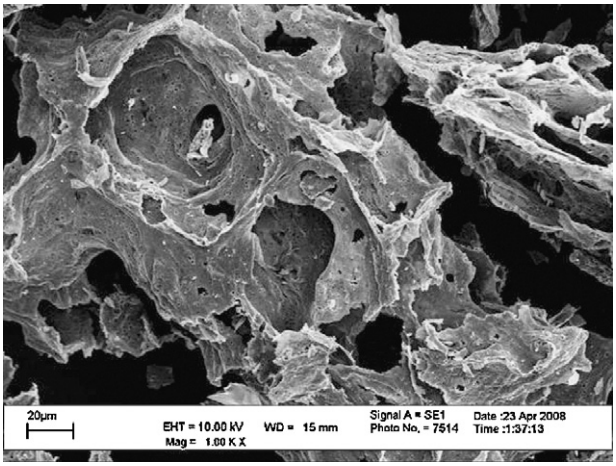

Fig. 6. SEM image of the powder calcined at 650 °C.

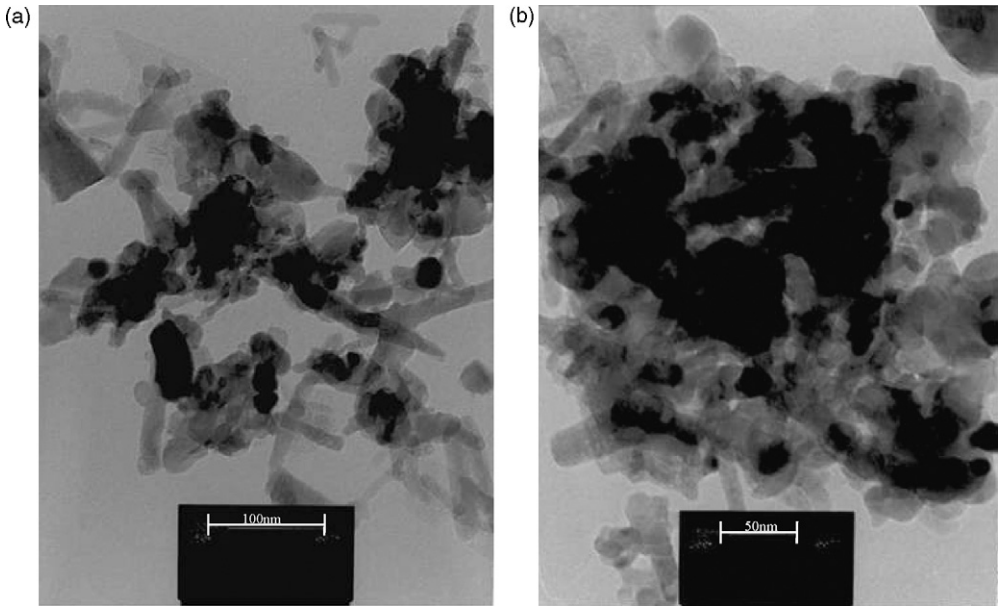

Fig. 7. (a) TEM image of powder calcined at 650 °C. (b) TEM image of powder calcined at 700 °C.

and A type phases were observed in the powders calcined at 650 and 700 °C. But except rhombohedral $LaNiO_3$ phase, there was no other phase in the samples calcined at 750 and 800 °C. The patterns showed broad diffraction peaks and those were attributed to the small size of the crystallites. The peak width decreased as the temperature of calcinations increased, which indicates that grain growth took place as the temperature increased.

Fig. 5 shows monotonic variation of crystallite size with the calcination temperature. It was observed that crystallite size increased from 14.63 to 17.56 nm when calcination temperature increased from 650 to 800 °C.

Band gap studies of the synthesized lanthanum nickelate powders calcined at 650 and 700 °C showed values 4.859 to 3.425 eV, respectively. On the other hand, the sample calcined at temperatures 750 and 800 °C showed no band gap. This indicates that the oxygen deficient tetragonal, monoclinic, triclinic and A type lanthanum nickelate phases are responsible for optical absorption in the UV–visible range of electromagnetic spectrum of light whereas the rhombohedral $LaNiO_3$ does not show any optical absorption in the said range, which revealed that this particular crystal structure is electronically conductive.

Fig. 6 shows the microstructure of as-calcined powder under scanning electron microscope. SEM study of the powder calcined at 650 °C revealed that the agglomerated powder is highly porous, which indicates the rapid evolution of gases during combustion.

TEM analysis shows that the crystallite sizes of powder calcined at 650 and 700 °C are 16–50 nm and 20–60 nm, respectively. Fig. 7a and b shows the TEM images for the powders calcined at 650 and 700 °C, respectively. The discrepancy between the crystallite diameter (14.63 and 17.56 nm) obtained from the XRD data and those (16–50 and 20–60 nm) from TEM is due to agglomeration among the primary particles.

4. Conclusion

Gel formed by heating a solution containing lanthanum(III) nitrate, nickel(III) nitrate and sucrose underwent self-sustaining smoldering type of combustion synthesis upon continued heating on a hot plate. The combustion was of complex nature, as evidenced by TGA–DSC plot. The TGA–DSC plot of the dried gel revealed that combustion reaction took place in two steps, one at 160 °C and the other at 350–525 °C. Variation in crystallite size was observed as the calcinations temperature increased, which was reflected in the values of specific surface area. TEM analysis revealed that hard agglomerates of the powder range from 20 to 60 nm. The powders calcined at different temperatures showed different behavior to optical absorption in the UV–visible range of optical spectrum, which is basically due to the various crystallographic structures. Phase pure rhombohedral $LaNiO_3$ can be used as electrode material since it has electronic conducting property. SEM study showed that sucrose combustion route produces highly agglomerated porous powder.

Acknowledgments

The author is grateful to Dr. J.N. Das, Director, NMRL, Dr. K. Prabhakaran, Mr. P.K. Ojha, Mr. Anand Melkeri and the colleagues of Ceramics Division of NMRL for their contribution in this work.

References

[1] N. Fujimura, H. Tanaka, H. Kitahata, H. Tadanaga, T. Yoshimura, T. Ito, Jpn. J. Appl. Phys. 36 (12A) (1997) L1601.
[2] N. Hamada, J. Phys. Chem. Solids 54 (10) (1993) 1157–1160.
[3] J.B. Torrance, P. Lacorre, A.I. Nazal, E.J. Ansaldo, Ch. Niedermayer, Phys. Rev. B 45 (1992) 8209.
[4] H. Yang, X. Zhang, W. Ao, G. Qiu, Mater. Res. Bull. 39 (2004) 833–837.
[5] L.N. Yannopoulos, Sensors Actuators 12 (3) (1987) 263–273.
[6] J.B. Goodenough, P.M. Raccah, J. Appl. Phys. 36 (1965) 1031.
[7] G. Demazeau, A. Marbeuf, M. Pouchard, P. Hagenmuller, J. Solid State Chem. 3 (1971) 582–589.
[8] A. Wold, B. Post, E. Banks, J. Am. Chem. Soc. 79 (1957) 4911.
[9] J.D.G. Fernandes, D.M.A. Melo, L.B. Zinner, C.M. Salustiano, Z.R. Silva, A.E. Martinelli, M. Cerqueira, C. Alves Junior, E. Longo, M.I.B. Bernardi, Mater. Lett. 53 (2002) 122–125.
[10] X. Weng, P. Boldrin, I. Abrahams, S.J. Skinner, S. Kellici, J.A. Darr, J. Solid State Chem. 181 (2008) 1123–1132.
[11] S.A. Nedilko, V.A. Kulichenko, A.G. Dziazko, E.G. Zenkovich, J. Alloys Compd. 367 (2004) 251–254.
[12] A.K. Norman, M.A. Morris, J. Mater. Process. Technol. 92–93 (1999) 91–96.
[13] J.K. Vassilion, M. Hornbostel, R. Ziebarth, F.J. Disalvo, J. Solid State Chem. 81 (1989) 208–216.
[14] P. Lacorre, J.B. Torrance, J. Pannetier, A.I. Nazzal, P.W. Wang, T.C. Huang, J. Solid State Chem. 91 (1991) 225–237.
[15] J. Brinker, G.W. Schere, Sol-Gel Science, Academic Press Publishing, Bristol and Philadelphia, 1988.
[16] T. Mimani, K.C. Patil, Mater. Phys. Mech. 4 (2001) 134–137.

[17] P.K. Ojha, K Pabhakaran, M. Biswas, T.K. Chongdar, N.M. Gokhale, S.C. Sharma, Adv. Appl. Ceram., in press.
[18] K. Deshpande, A. Mukasyan, A. Varma, J. Am. Ceram. Soc. 86 (2003) 1149.
[19] L.A. Chick, L.R. Pederson, G.D. Maupain, J.L. Bates, L.E. Thomas, G.J. Exarhos, Mater. Lett. 10 (1990) 6–12.
[20] M. Biswas, K. Shashidhara, P.K. Ojha, T.K. Chongdar, N.R. Bandyopadhyay, J. Am. Ceram. Soc. 91 (3) (2008) 934–937.
[21] M. Biswas, K. Prabhakaran, N.M. Gokhale, S.C. Sharma, Mater. Res. Bull. 42 (4) (2007) 609–617.
[22] I. Ganesh, B. Srinivas, R. Johnson, B.P. Saha, Y.R. Mahajan, Brit. Ceram. Trans. 101 (2001) 247–254.
[23] S. Bose, A. Banerjee, J. Am. Ceram. Soc. 87 (2004) 487–489.
[24] S. Bose, S.K. Saha, J. Am. Ceram. Soc. 86 (2003) 1055–1057.
[25] S. Bose, Y. Wu, J. Am. Ceram. Soc. 88 (2005) 1999–2002.
[26] K. Prabhakaran, N.M. Gokhale, S.C. Sharma, R. Lal, Ceram. Int. 31 (2005) 327–332.
[27] R.S. Guo, Q.T. Wei, H.L. Li, F.H. Wang, Mater. Lett. 60 (2006) 261.
[28] J. Zhang, J. Ning, X. Liu, Y. Pan, L. Huang, Mater. Res. Bull. 38 (2003) 1249.
[29] X. Qi, J. Zhou, Z. Yue, Z. Gui, L. Li, Mater. Chem. Phys. 78 (2003) 25.
[30] R.D. Purohit, A.K. Tyagi, J. Mater. Chem. 12 (2002) 312.
[31] C. Laberty-Robert, F. Ansart, C. Deloget, M. Gaudon, A. Rousset, Ceram. Int. 29 (2003) 151.
[32] T. He, Q. He, N. Wang, J. Alloys Compd. 396 (2005) 299.
[33] N.T.H. Le, J.M. Calderón-Moreno, M. Popa, D. Crespo, L.V. Hong, N. Phuc, J. Eur. Ceram. Soc. 26 (2006) 403–407.
[34] Y. Wang, J. Zhu, X. Yang, L. Lu, X. Wang, Mater. Res. Bull. 41 (8) (2006) 1565–1570.
[35] B.D. Culity, Elements of X-Ray Diffraction, Addison-Wesley, Reading, MA, 1978.
[36] J.M. González-Calbet, M.J. Sayagués, M. Vallet-Regí, Solid State Ion. 32–33 (1989) 721–726.
[37] E.F. Bertaut, L. Blum, A. Sagnieres, Acta Crystallogr. 12 (1959) 149.
[38] J.C. Grenier, M. Pouchard, P. Hagenmuller, P., Structure and Bonding, Vol. 47, Springer, Berlin, 1981, p. 1.
[39] J.M. González-Calbet, M.A. Vallet-Regi, J. Solid State Chem. 68 (1987) 266.